Research on the Optimal Detection Timing for NIPT Based on Segmented Risk Modeling and Simulated Annealing Optimization

Zhiyu Wang[1,a,*]

[1]School of Economics and Management, China University of Geosciences (Wuhan), Wuhan, China

[a]m18631934910@163.com

[*]Corresponding author

Keywords: Non-invasive prenatal testing (NIPT); BMI segmentation; generalized additive model (GAM); risk function; simulated annealing; female fetus abnormality classification

Abstract: Non-invasive prenatal testing (NIPT) has become an important tool in prenatal screening, yet the question of "when to test for the best outcome" in clinical practice still largely relies on rule-of-thumb time windows, and the impact of individual differences—especially maternal BMI—on testing effectiveness is often underestimated. This study proposes an individualized framework for determining the testing time that proceeds from dependence identification, nonlinear modelling, segmented risk evaluation, and global optimization." We first use Spearman correlation and distance correlation to characterize the dependence structure between key variables and Y-chromosome concentration, and then adopt a generalized additive model (GAM) to obtain an interpretable nonlinear baseline. Building on this, we derive optimal BMI segments via dynamic programming on model residuals, and construct an integrated risk function that simultaneously covers false negatives, false positives, and test failure, while incorporating a gestational-age penalty and an adjustment factor for "attainment status." Finally, we perform a global search with simulated annealing over the feasible gestational window to obtain the optimal testing time for each segment. Empirical results show that, under the baseline scenario, the optimal testing times for the six BMI groups cluster around 10.0–11.7 weeks, which are overall substantially earlier than the actual testing weeks (by about 4.4–8.4 weeks). Risk decomposition indicates that the delay penalty dominates, and test-failure risk is higher in high-BMI groups. Under multiple error scenarios of light/moderate/severe perturbations, the optimal time essentially converges to around 10.0 weeks, indicating robust decision-making. For female-fetus samples, the constructed SVM classifier achieves an AUC of 0.9550 without relying on Y-chromosome information. The framework provides a reproducible and practical quantitative basis for individualized NIPT testing-time recommendations and female-fetus abnormality classification.

1. Introduction

Non-invasive prenatal testing (NIPT)[1], [2] analyzes fetal cell-free DNA in maternal peripheral blood through high-throughput sequencing to screen for common chromosomal aneuploidies at an early stage. Because of its safety and its high sensitivity and specificity, it has been widely used in clinical practice. However, the selection of testing time often follows a "one-size-fits-all window" rooted in experience, which fails to adequately reflect individual differences—particularly the impacts of maternal BMI[3], [4], gestational progression, and sequencing quality control indicators on the "attainment probability" and interpretive stability.

Existing studies generally proceed along two paths. One line emphasizes biological priors centered on "fetal fraction/attainment thresholds," supplemented by linear or semiparametric models to adjust for the effects of gestational age and maternal characteristics. The other introduces machine-learning models to directly model the probabilities of positive/negative outcomes and failure using multi-source features, with the testing time chosen by empirical or heuristic criteria. The former has advantages in interpretability but is limited in its ability to capture nonlinear and non-monotonic effects; the latter has stronger predictive power but often lacks a decision-

  DOI: 10.25236/iwmecs.2025.014

quantification framework that can directly connect to clinical costs.

To address these shortcomings, this paper proposes, on a real clinical dataset, an integrated "statistics–learning–optimization" solution: use distance correlation and GAM[5], [6] to clarify the nonlinear roles of key variables; implement data-driven BMI segmentation via dynamic programming on residuals; construct an integrated risk function—"false negative/false positive/test failure + gestational-age penalty + attainment status"—that directly maps to clinical costs; and directly minimize this risk over the feasible gestational window via simulated annealing to obtain individualized optimal testing times for each segment. Furthermore, recognizing the inevitability of technical perturbations such as fluctuations in read depth, GC bias, and alignment rate, we define error scenarios of varying intensities under the same estimator to evaluate the stability of the optimal plan. Meanwhile, for the challenge of female-fetus classification without Y-chromosome information, we build an SVM-based classifier using multi-source features to complete the application pipeline. The overall framework yields the following highlights in experiments: BMI is automatically partitioned into six segments; under the baseline, optimal times concentrate around 10–12 weeks and are overall earlier than the actual testing time; the delay penalty is the dominant risk component; test-failure risk is higher in high-BMI groups; under error scenarios, optimal times robustly converge to around 10 weeks; and the female-fetus classifier attains a high AUC with interpretable importance clues. Collectively, these results indicate that, compared with a fixed window, individualized timing recommendations can significantly reduce overall risk without compromising classification performance, providing a basis for optimizing clinical workflows.

2. Methods

2.1 Data Preprocessing and Label Construction

After standardizing fields, denoising, and handling missing values in the raw data, we unify measurement units and apply logarithmic/standardization transforms to skewed continuous variables to alleviate heteroskedasticity. Centered on the three types of events that need to be modeled in subsequent risk evaluation, we construct binary labels:

$$Y_{\mathrm{FN}} = \mathbf{1}\{\text{Genetically abnormal but NIPT indicates healthy }\} \tag{1}$$

$$Y_{\mathrm{FP}} = \mathbf{1}\{\text{Healthy but NIPT indicates abnormality }\} \tag{2}$$

$$Y_{\mathrm{fail}} = \mathbf{1}\{\text{Detection invalid}\} \tag{3}$$

used to estimate $\hat{P}_{\mathrm{FN}}, \hat{P}_{\mathrm{FP}}, \hat{P}_{\mathrm{fail}}$. At the same time, we retain the "valid detection probability" $\hat{P}_{\mathrm{valid}}$ and the gestational-age penalty and attainment adjustment factor needed subsequently in the risk-function components so they can be linked within a unified framework.

2.2 Dependence Identification and GAM Modeling

To identify the dependence structure between key covariates and the response, we first characterize monotonic relationships with Spearman's rank correlation, and then test for more general (including nonlinear and non-monotonic) dependence using distance correlation (dCor). The definition of dCor is:

$$\mathrm{dCor}(X,Y) = \frac{\mathrm{dCov}(X,Y)}{\sqrt{\mathrm{dVar}(X)\,\mathrm{dVar}(Y)}} \in [0,1] \tag{4}$$

which equals 0 if and only if the variables are independent, compensating for the blind spot of rank correlation with respect to non-monotonic patterns. With multiple-testing correction and interval estimation, we use dCor to confirm significant nonlinear dependence between gestational age, BMI, age, fetal-health[7], [8] indicator, etc., and concentration, with X-chromosome concentration most strongly associated with concentration (see Table 1), laying the groundwork for subsequent nonlinear modeling.

Table 1: Significance test results of distance correlation coefficients

Variable	dCor	95% CI	Effect size	Significance
X-chromosome concentration	0.514	[0.465, 0.561]	Large	***
Maternal BMI	0.165	[0.123, 0.223]	Small	***
Age	0.145	[0.109, 0.201]	Small	***
Gestational age	0.129	[0.106, 0.181]	Small	***
Fetal health (yes/no)	0.126	[0.074, 0.177]	Small	***
IVF pregnancy	0.072	[0.032, 0.120]	Very small	*
Parity	0.070	[0.058, 0.120]	Very small	ns
Gravidity	0.068	[0.052, 0.121]	Very small	ns

Accordingly, we adopt a generalized additive model (GAM) to capture the nonlinear effects of key variables on while retaining interpretability. The model is:

$$\mathbb{E}[\log(V)] = \beta_0 + f_1(C) + f_2(J) + f_3(K) + f_4(W) + \beta_5 AE \tag{5}$$

Where V is Y-chromosome concentration; C is age; J is gestational age at testing; K is BMI; W is X-chromosome concentration; AE is the fetal-health indicator. The are spline smoothers (the basis size of each smoother is given in the text) used to flexibly fit nonlinear effects.

2.3 Segmented Risk Modeling and Global Optimization

2.3.1 Optimal BMI Segmentation Based on GAM Residuals

Within the GAM framework of Section 2.2, let the residual be $e = \log(V) - \hat{m}(C, J, K, W, AE)$. As shown in Figure 1, the "residual–BMI" relationship exhibits systematic shifts in certain regions of K, necessitating segmentation.

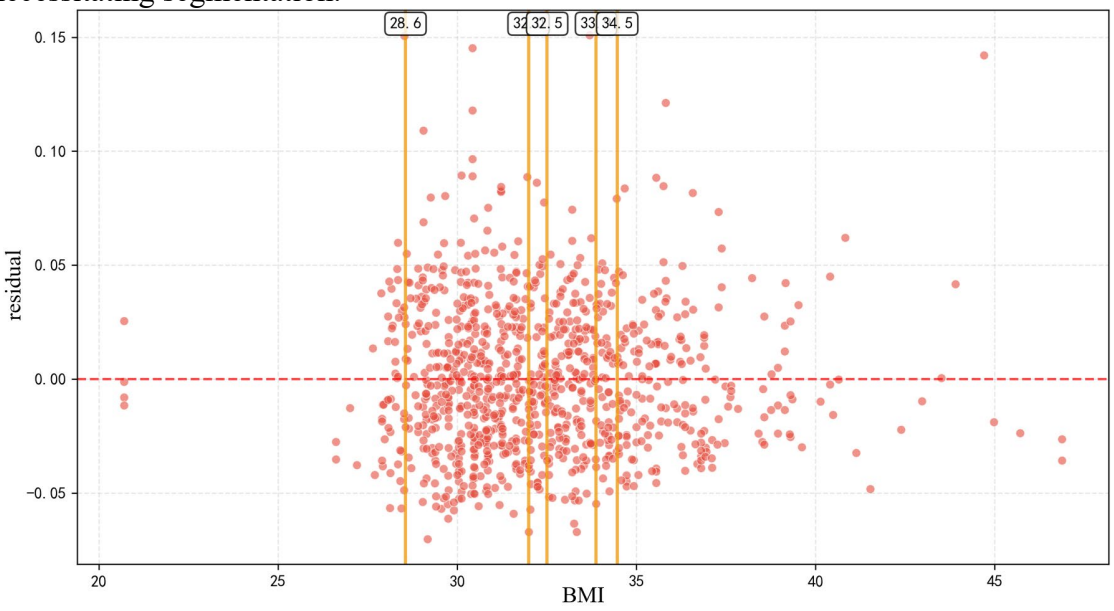

Figure 1 Residual vs. BMI

Let the breakpoints $b_0 < b_1 < \cdots < b_K < b_{K+1}$ be (the endpoints are the sample minimum/maximum BMI). For any interval $[b_i, b_j)$, define the cost:

$$\text{cost}(i,j) = \underbrace{\text{Var}\left(e \mid K \in [b_i, b_j)\right)}_{\text{Intra-segment residual variance}} + \alpha \underbrace{\int_{b_i}^{b_j} \left\{\frac{\mathrm{d}}{\mathrm{d}K}\hat{\mu}_e(K)\right\}^2 \mathrm{d}K}_{\text{Roughness Penalty on Residual Mean Curves}} \tag{6}$$

Under the constraints of a maximum number $K_{\max}$ of segments and an additional segment penalty γ, we solve the dynamic programming problem:

$$\min_{K \le K_{\max}, \{b_r\}} \sum_{r=0}^{K} \text{cost}(r, r+1) + \gamma K \tag{7}$$

and obtain the optimal set of breakpoints via backtracking.

2.3.2 Unified Characterization of the Risk Function

Given BMI segment K and gestational age J, define the integrated risk:

$$R(J \mid K) = [\lambda_{\mathrm{FN}}\hat{P}_{\mathrm{FN}}(J,K) + \lambda_{\mathrm{FP}}\hat{P}_{\mathrm{FP}}(J,K) + \lambda_{\mathrm{fail}}(1 - \hat{P}_{\mathrm{valid}}(J,K))] \cdot \mathrm{RiskPenalty}(J) \cdot \mathrm{AdjustmentFactor} \quad (8)$$

where $\lambda_\cdot > 0$ denotes the relative cost weights for error types/failure, $\mathrm{RiskPenalty}(J)$ represents the gestational-age penalty for delayed testing, and $\mathrm{AdjustmentFactor}$ is the adjustment factor based on the "attainment status" of Y concentration, as shown in Figure 2. This expression provides a unified measure—across BMI segments—of the risk differences induced by "when to test," and serves as the objective for the subsequent search for the optimal time.

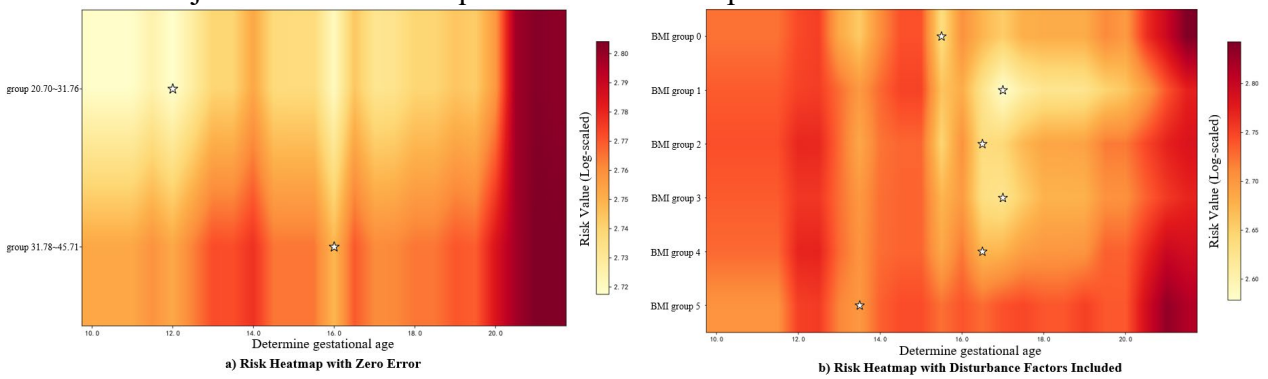

Figure 2 Comparison of risk heatmaps for optimal testing time across BMI groups under different error conditions (white asterisks indicate the optimal testing time)

2.3.3 Estimation of Probability Terms and Segment-Level Aggregation

$\hat{P}_{\mathrm{FN}}, \hat{P}_{\mathrm{FP}}, \hat{P}_{\mathrm{fail}}, \hat{P}_{\mathrm{valid}}$ are approximated via supervised learning using a gradient-boosting implementation that performs binary probability estimation on features such as $(J, K, C, W, \dots)$. Within each BMI segment, for a given gestational age, we average (or robustly average) individual predicted probabilities for substitution into the components of $R(J \mid K)$. This approach leverages high-dimensional nonlinear structure without sacrificing interpretability and facilitates updates across segments.

2.3.4 Simulated Annealing Search for the Globally Optimal Testing Time

Given BMI segment K and risk function $R(J \mid K)$, over the feasible gestational window $J \in [\underline{J}, \bar{J}]$, we use simulated annealing (SA) to find the global minimizer:

$$J^{\star} = \arg\min_{J \in [\underline{J}, \bar{J}]} R(J \mid K) \quad (9)$$

Where $R(J \mid K)$ plays the role of the energy, so we write $E(J) = R(J \mid K)$.

Set the initial temperature $T_0 > 0$, terminal temperature $T_{\min} > 0$, and geometric cooling factor $\alpha \in (0,1)$. Randomly draw a starting point $J_{\mathrm{current}} \sim \mathrm{Unif}([\underline{J}, \bar{J}])$ within the feasible domain and compute the current energy $E_{\mathrm{current}} = R(J_{\mathrm{current}} \mid K)$. Simultaneously set to store the best solution found so far and its energy. The main loop starts with $T \leftarrow T_0$ and terminates when $T \le T_{\min}$.

At each temperature level T, generate a candidate from the neighborhood of the current solution,

$$J_{\mathrm{new}} = \Pi_{[\underline{J}, \bar{J}]}\,(J_{\mathrm{current}} + \delta \cdot \varepsilon), \varepsilon \sim \mathcal{N}(0,1) \quad (10)$$

where Π is a projection (or clipping) operator enforcing the gestational bounds, and $\delta > 0$ is a step-size factor that can be linked to the temperature (in implementation, is used, with clipping/projection to [10,22] weeks). Then compute $E_{\mathrm{new}} = R(J_{\mathrm{new}} \mid K)$. This neighborhood and clipping strategy is based on a "neighborhood perturbation + clip" implementation.

If the candidate improves the objective ($E_{\text{new}} < E_{\text{current}}$), accept it unconditionally; otherwise, accept the "worse" solution with probability:

$$p_{\text{acc}} = \exp\left(-\frac{E_{\text{new}} - E_{\text{current}}}{T}\right) = \exp\left(\frac{E_{\text{current}} - E_{\text{new}}}{T}\right) \tag{11}$$

After acceptance, update $(J_{\text{current}}, E_{\text{current}}) \leftarrow (J_{\text{new}}, E_{\text{new}})$, and refresh the global best pair. This criterion allows "uphill moves" with higher probability at high temperature to escape local minima; as temperature decreases, the probability of accepting worse solutions decays exponentially.

Update the temperature geometrically $T \leftarrow \alpha T$, until $T \leq T_{\min}$, then output the recorded optimal gestational age. The implementation also provides an equivalent termination in terms of a maximum number of iterations $N_{\max}$: let:

$$T_i = T_0\left(\frac{T_{\min}}{T_0}\right)^{i/N_{\max}} \ (i = 0, \ldots, N_{\max}) \tag{12}$$

so that after exactly perturbations, the temperature reaches $T_{\min}$.

Considering the non-convexity of $R(J \mid K)$ and the numerical noise in the probability terms $\hat{P}_{\text{FN}}, \hat{P}_{\text{FP}}, \hat{P}_{\text{fail}}$, we repeat SA multiple times (default 3) for each BMI segment, retaining the run with the smallest risk. If multiple runs still fail to produce a usable solution, we fall back to a uniform grid search to ensure a feasible solution exists.

Each "energy" evaluation in SA is computed via $E(J) = R(J \mid K)$: first obtain the probability terms from the learner, then assemble the risk and multiply by the gestational-age penalty. Hence the computational complexity of SA is dominated by the cost of a single risk evaluation, with overall complexity $\mathcal{O}(N_{\max} \times \text{cost}[R])$.

2.3.5 Perturbation by Testing-Error Scenarios and Robustness Evaluation

Recognizing that fluctuations in read depth, GC bias, and alignment rate may alter $\hat{P}$ and $\hat{P}_{\text{valid}}$, we apply random perturbations of layered intensity (light/moderate/severe) to the input features under the same estimator, substitute the updated probabilities into $R(J \mid K)$, and repeat the SA search to compare the stability of $J^{\star}$ under different scenarios.

2.4 Extended Model for Abnormality Classification in Female Fetuses (SVM)

Because female fetuses lack information, we construct an independent classifier that does not rely on . We first use the F-test (ANOVA) for feature screening across multi-dimensional clinical and sequencing features; then we train a nonlinear SVM[9], [10] for classification; we extract interpretable rules via a decision tree; and finally, we form a three-tier risk-classification procedure through threshold optimization.

3. Experiments and Results

Building on the model specification and derivations in Chapter 2, this chapter presents the data overview, baseline optimal testing times, the composition of risk and its evolution with gestational age, robustness under error scenarios, and empirical results for the female-fetus extended classifier. The numbering of figures and tables follows the original manuscript for cross-reference. For consistency with Chapter 2, we retain the previously defined notation and segmentation scheme.

3.1 Data Description

After GAM modeling and residual analysis, optimal segmentation of BMI into six groups was determined via dynamic programming: (20.7,28.6], (28.6,32.0], (32.0,32.5], (32.5,33.9], (33.9,34.5], (34.5,46.9] ; systematic shifts in residuals versus BMI appear in the 28–35 range, validating the need for segmentation, as shown in Figures 3, 4, and 5.

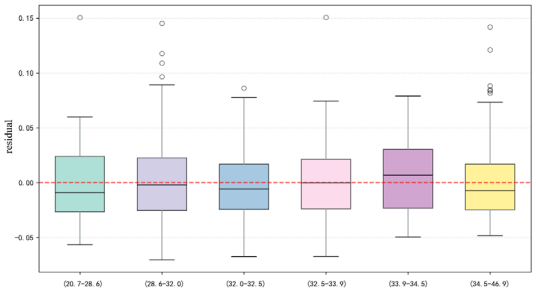

Figure 3 Boxplots of residuals by segment

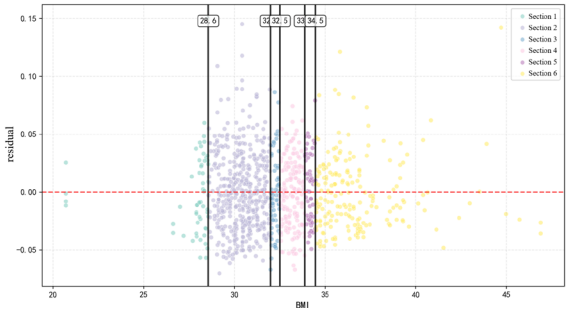

Figure 4 Residual vs. BMI (with segmentation lines)

The sample size, BMI range, and average BMI for each segment are also used for subsequent risk aggregation and optimal-time calculation.

3.2 GAM Fitting and Key Variable Effects

Following dependence screening, the original manuscript fits with a GAM using the nonlinear/linear combination of age, gestational age , BMI , X-chromosome concentration , and fetal-health indicator , with smoother basis sizes of , and provides detailed spline coefficients as shown in Table 2.

Table 2 Detailed spline coefficients of the GAM

Variable	Spline coefficients (in order of basis functions)
Age C	0.0194,-0.0092,0.0103,0.0017,0.0044,0.0016,-0.0053,0.0012,-0.0134,-0.0018,0.0196,0.0218,-0.0020,-0.0310,0.0056
Gestational Age J	-0.0029,-0.0035,0.0177,-0.0024,0.0155,-0.0088,-0.0020,0.0143,0.0209,0.0168,0.0113,0.0049,-0.0100
Maternal BMI K	-0.0016,0.0075,0.0201,0.0347,0.0170,0.0229,0.0158,0.0024,0.0092,0.0145,-0.0075,-0.0375,-0.0468
X Chromosome Concentration W	-0.0539,-0.0511,-0.0253,-0.0121,0.0388,0.0917,0.1460,0.0029
Fetal Health AE	0.0875

3.3 Baseline Optimal Testing Time

Under the “no-error baseline” scenario, combining XGBoost probability estimates with the risk function and using simulated annealing to search across BMI segments yields the optimal NIPT testing time and corresponding minimum risk values shown in Table 3: for groups 1–6, the optimal weeks are approximately 11.1, 10.6, 11.6, 11.7, 10.9, and 10.0; the corresponding minimum risks are 2.3048, 1.9194, 2.1283, 2.7160, 1.0201, and 1.8519. Compared with the actual testing weeks, these optimal times are generally earlier by 4.4–8.4 weeks; the highest-BMI group (group 6) has the earliest recommendation (10.0 weeks) and the largest improvement (8.4 weeks). In addition, BMI and the optimal testing time show a moderate negative correlation (), suggesting earlier testing for higher BMI.

Table 3 Baseline optimal NIPT testing time by BMI group

Group	BMI Range	Sample Size	Average BMI	Actual Post-Pregnancy	Optimal Timing	Risk Value	Improvement (Weeks)
1	≤28.6	57	27.6	16.6	11.1	2.3048	-5.6
2	(28.6,32.0)	456	30.4	16.8	10.6	1.9194	-6.2
3	(32.0,32.5)	66	32.2	16.6	11.6	2.1283	-5.0
4	(32.5,33.9)	164	33.2	16.2	11.7	2.7160	-4.4
5	(33.9,34.5)	55	34.2	16.0	10.9	1.0201	-5.0
6	>34.5	197	36.8	18.4	10.0	1.8519	-8.4

3.4 Composition of Risk and Its Evolution with Gestational Age

To explain the above optimal times, the manuscript decomposes the integrated risk into components (delay penalty, false negative, false positive, and test failure). Figure 5 shows that the delay penalty dominates across groups (average contribution >60%); the test-failure risk is higher in high-BMI groups (groups 4 and 6), consistent with clinical experience.

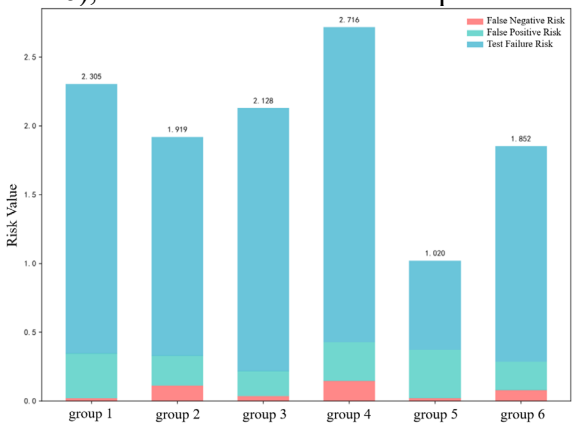

Figure 5 Decomposition of risk components by BMI segment

3.5 Robustness under Error Scenarios

Accounting for technical fluctuations in read depth, GC bias, and alignment rate, three error scenarios—light, moderate, and severe—are defined. Features are perturbed accordingly while reusing the same estimator and optimization flow. Results are shown in Table 4: the optimal time in nearly all BMI groups shifts to 10.0 weeks (groups 1–5 move earlier by about 1.1, 0.6, 1.6, 1.7, and 0.9 weeks, respectively, relative to the baseline; group 6 remains at 10.0), indicating a high degree of consistency under error.

Table 4. Changes in optimal NIPT testing time under different error scenarios

BMI Grouping	Baseline		Minor error		Moderate error		Severe error	
	Time	Risk Value	time	△week	time	△week	time	△week
1	11.1	2.3048	10.0	-1.1	10.0	-1.1	10.0	-1.1
2	10.6	1.9194	10.0	-0.6	10.0	-0.6	10.0	-0.6
3	11.6	2.1283	10.0	-1.6	10.0	-1.6	10.0	-1.6
4	11.7	2.7160	10.0	-1.7	10.0	-1.7	10.0	-1.7
5	10.9	1.0201	10.0	-0.9	10.0	-0.9	10.0	-0.9
6	10.0	1.8519	10.0	0.0	10.0	0.0	10.0	0.0

3.6 Extended Model for Female-Fetus Abnormality Classification

On female-fetus samples without information, an SVM classifier is trained and reports ROC AUC = 0.9550, indicating good classification performance, as shown in Figure 6.

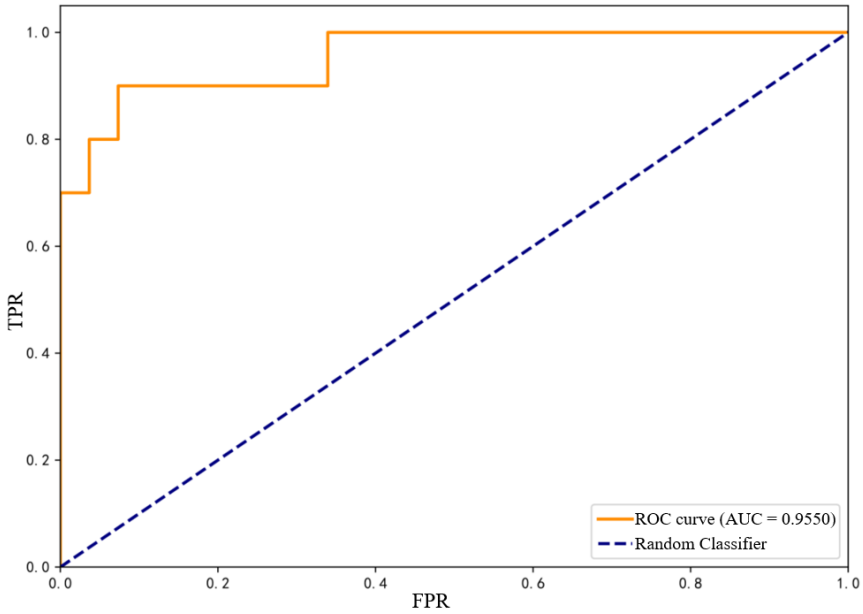

Figure 6 ROC curve

With the accompanying sensitivity analysis, the 18-chromosome value contributes the most, followed by the X- and 13-chromosome values, providing a basis for rule extraction and threshold optimization.

4. Conclusion

This study addresses two core questions for NIPT "when to test for the best outcome" and "how to classify abnormalities in female fetuses"—by proposing an individualized decision framework built on nonlinear statistical modeling, segmented risk metrics, and global optimization. Empirical results show that, on real data, the six BMI segments derived from residuals effectively alleviate systematic bias of a single model across populations. The integrated risk function organically combines false negatives, false positives, and test failures with a gestational-age penalty and attainment status, enabling the testing time to be directly tied to clinical costs in an interpretable way. On this basis, simulated annealing yields optimal testing times concentrated in 10.0–11.7 weeks, significantly earlier than actual testing gestational ages, and exhibiting high consistency across multiple error scenarios. The female-fetus extension attains an AUC of 0.9550 without relying on Y-chromosome information, completing applicability across fetal sexes. We emphasize that limitations remain: the setting of weight and penalty parameters requires further prospective clinical evidence; data sources and population composition may affect generalizability. Future work can pursue external validation on multi-center data, clinical calibration of cost weights, deeper integration into physician workflows, and multimodal fusion with ultrasound and metabolic indicators. Overall, this paper presents a reusable, interpretable, and noise-robust path to individualized determination of NIPT testing time and provides an effective supplement for female-fetus classification, with potential for clinical translation.

References

[1] D. Kim, J. Y. Sohn, J. H. Cho, J.-H. Choi, G.-Y. Oh, and H. G. Woo, "KF-NIPT: K-mer and fetal fraction-based estimation of chromosomal anomaly from NIPT data," *BMC Bioinformatics*, vol. 26, no. Compendex, 2025

[2] X. Ge, Z. Yao, and Y. Du, "Medical priority fusion: achieving dual optimization of sensitivity and interpretability in nipt anomaly detection," Sept. 22, 2025, arXiv: arXiv:2509.17924. doi: 10.48550/arXiv.2509.17924.

[3] K. Gunawan, E. Fachrial, A. Amansyah, and B. Halim, "Association between Body Mass Index

(BMI) and DNA Fragmentation Index," in *2021 IEEE International Conference on Health, Instrumentation and Measurement, and Natural Sciences, InHeNce 2021, July 14, 2021 - July 16, 2021*, Virtual, Medan, Indonesia: Institute of Electrical and Electronics Engineers Inc., 2021.

[4] L. A. AL Raheim Hamza, H. A. Lafta, and S. Z. Al Rashid, "Classification of DNA Sequence for Diabetes Mellitus Type Using Machine Learning Methods," in *7th International Conference on Microelectronics and Telecommunication Engineering, ICMETE 2023, September 22, 2023 - September 23, 2023*, in Lecture Notes in Networks and Systems, vol. 894. Ghaziabad, India: Springer Science and Business Media Deutschland GmbH, 2024, pp. 87–102.

[5] L. Lu, Z. Si, Z. Liu, and T. Mei, "Big-Data-driven Part Anomaly Detection under Smart Manufacturing: A Study based on GAM–Boost Technology," *Journal of Imaging Science and Technology*, vol. 69, no. Compendex, 2025.

[6] Y. Wang and Y. Wang, "Research on Micro-expression Recognition Based on GAM Attention Mechanism and Transfer Learning," in *4th Asia-Pacific Conference on Communications Technology and Computer Science, ACCTCS 2024, February 24, 2024 - February 26, 2024*, Shenyang, China: Institute of Electrical and Electronics Engineers Inc., 2024, pp. 350–355.

[7] D. Sudharson, V. Sushmita, P. Jananiksha, V. Vaishali, R. Mukilarasu, and S. Kanagaraj, "AI Powered Monitoring and Risk Prediction for Maternal Health to Ensure Fetal Well-Being," in *3rd International Conference on Advancements in Electrical, Electronics, Communication, Computing and Automation, ICAECA 2025, April 4, 2025 - April 5, 2025*, Hybrid, Coimbatore, India: Institute of Electrical and Electronics Engineers Inc., 2025.

[8] G. Rohini, D. Harini, R. Vaishnavi, and C. Mohan, "Enhanced Fetal Health Monitoring: Implementation of Django Server for Comprehensive Tracking and Analysis," in *2025 IEEE Bangalore Humanitarian Technology Conference, B-HTC 2025, April 25, 2025 - April 26, 2025*, Belagavi, India: Institute of Electrical and Electronics Engineers Inc., 2025.

[9] S. Sardesai and R. Gedam, "Hybrid EEG Signal Processing Framework for Driver Drowsiness Detection Using QWT, EMD, and Bayesian Optimized SVM," in *3rd International Conference on Integrated Circuits and Communication Systems, ICICACS 2025, February 21, 2025 - February 22, 2025*, Hybrid, Raichur, India: Institute of Electrical and Electronics Engineers Inc., 2025.

[10] L. Chang *et al.*, "Research on Prediction Model Based on Hybrid Algorithm of PSO-SVM Kernel Function," in *7th International Conference on Artificial Intelligence Technologies and Applications, ICAITA 2025, June 27, 2025 - June 29, 2025*, Wenzhou, China: Institute of Electrical and Electronics Engineers Inc., 2025.